

Variability of the thermohaline structure and transport of Atlantic water in the Arctic Ocean based on NABOS CTD data

Nataliya Zhurbas¹ and Natalia Kuzmina¹


¹Shirshov Institute of Oceanology, Russian Academy of Sciences, 36 Nakhimovsky Prospekt ,
5 117997 Moscow, Russia

Correspondence to: Nataliya Zhurbas (nvzhurbas@gmail.com)

Abstract. CTD transects across continental slope of the Eurasian Basin and the St. Anna Trough performed during NABOS (Nansen and Amundsen Basins Observing System) project in 2002–2015 are used to describe θ - S characteristics and volume flow rates of the current carrying the Atlantic Water (AW) in the Arctic Ocean. The CTD dataset includes 33 sections in the Eurasian Basin, 4 transects in the St. Anna Trough and 2 transects in the Makarov Basin; additionally a CTD transect of the Polarstern-1996 expedition (PS-96) is used. The variability of thermohaline pattern on the AW pathway along the slope of Eurasian Basin is investigated. The Fram Strait branch of the Atlantic Water (FSBW) is identified on all transects, including two transects in the Makarov Basin (along 159°E), while the cold waters, which can be associated with the influence of the Barents Sea branch of the Atlantic water (BSBW), on the transects along 126°E, 142°E and 159°E, were observed in the depth range below 800 m and had a negligible effect on the spatial structure of isopycnic surfaces. An interpretation of the spatial and temporal variability of hydrological parameters characterizing the flow of the AW in the Eurasian Basin is presented. The geostrophic volume transport of AW decreases farther away from the areas of the AW inflow to the Eurasian Basin, decreasing by one order of magnitude in the Makarov Basin at 159°E, implying that the major part of the AW entering the Arctic Ocean circulates cyclonically within the Nansen and Amundsen Basins. There is an absolute maximum of θ_{max} (AW core temperature) in 2006–2008 time series and a maximum in 2013, but only at 103°E. Salinity $S(\theta_{max})$ (AW core salinity) time series display an increase of the AW salinity in 2006–2008 and 2013 (at 103°E) that can be referred to as a AW salinization in the early 2000s. The maxima of θ_{max} and $S(\theta_{max})$ in 2006 and 2013 are accompanied by the volume transport maxima. The time average geostrophic volume transports of AW, V_{mean} , are $V_{mean} = 0.5$ Sv in the longitude range 31–92°E, $V_{mean} = 0.8$ Sv in the St. Anna Trough and $V_{mean} = 1.1$ Sv in the longitude range 94–30 107°E.

1 Introduction

Atlantic water (AW) enters the Eurasian Basin by two branches (see, e.g., Aagaard, 1981; Rudels et al., 1994; Schauer et al., 1997; Rudels et al., 1999; Schauer et al., 2002a, b; Rudels et al., 2006; Berzczynska-Möller et al., 2012; Rudels et al., 2015; Rudels, 2015; Dmitrenko et al., 35 2015; Pnyushkov et al., 2015, 2018b): one of them originates from the Greenland and Norwegian seas and flows to the basin through the Fram Strait (Fram Strait branch of the Atlantic Water, hereinafter the FSBW), and the other reaches the deep part of the Arctic Ocean near St. Anna Through after passing through the Barents Sea (Barents Sea branch of the Atlantic water, hereinafter the BSBW). After entering the Eurasian Basin the FSBW moves eastward with the 40 subsurface boundary current and has a core of higher temperature and salinity. In the longitude range of 80–90°E it encounters and partially mixes with the BSBW, which is strongly cooled due to mixing with shallow waters of the Arctic shelf seas and atmospheric impact (Schauer et al., 1997; 2002a, b). Further, the water masses resulting from the interaction of two branches which transport the AW continue spreading cyclonically in the Eurasian Basin.

 To study the characteristics of the FSBW and BSBW flow in the Eurasian Basin, it is useful to estimate, first of all, its volume flow rate in different parts of the basin. Generally the estimates of the AW volume flow rate have been based on direct current observations (Fahrbach et al., 2001; Berzczynska-Möller et al., 2012; Rudels et al., 2014; Pnyushkov et al., 2015). However, it is useful also to consider the AW geostrophic volume flow rate calculated on the basis of CTD 50 data. Such estimates, obtained for different regions of the Arctic Ocean, were given in a number of papers (e.g. Marnela et al., 2013; Våge et al., 2016; Pérez-Hernández et al., 2017; Kolås and Fer, 2018). For completeness, it is of interest to carry out estimates of the AW geostrophic volume flow rate along continental slope of the Eurasian Basin based on a large volume of empirical data.

55 Within the NABOS (Nansen and Amundsen Basins Observing System) project (Polyakov et al., 2007) a unique volume of CTD data was collected: more than 30 sections were made in various regions of the Arctic Basin in the summer/fall 2002-2015. A number of sections in different years were made in the same regions of the Basin, which allows studying the interannual variability of the water masses thermohaline structure and the geostrophic volume 60 flow rate in these areas.

The main goal of this work is to investigate the spatial and temporal variability of the AW geostrophic volume flow rate during its propagation along the continental slope of the Eurasian Basin. Another important aspect of our analysis is the investigation of the thermohaline structure and transformation of the FSBW and BSBW. Such analysis is essential for two reasons: a) the 65 estimates of the AW transport are sensitive to the temperature and salinity ranges used for the

identification of this water (Pnyushkov et al., 2018b); b) it is reasonable to assume that mixing of FSBW, BSBW and surrounding waters may change the AW geostrophic volume flow rate.

2 Material and Methods

We used data of CTD profiling on transects across the slope of the Eurasian Basin in the longitude range of 31–159°E measured in the years 2002–2015 within the framework of NABOS project (in total 39 transects). The data are freely available at the site <http://nabos.iarc.uaf.edu>. In addition, a CTD transect across the entire Eurasian Basin and over the Lomonosov Ridge starting at 92°E at the slope from R/V *Polarstern* in 1996 (hereafter PS96) was also included. The locations of the CTD transects are shown in Fig. 1. It can be seen from the map in Fig. 1 that most of the CTD transects are aligned cross-slope and grouped at longitudes of 31, 60, 90, 92, 94, 96, 98, 103, 126, 142, and 159°E. Four of the 40 transects crossed zonally the St. Anna Trough (at the latitude of 81, 81.33, 81.42, and 82°N) through which the BSBW enters the Eurasian Basin. Most of the CTD casts covered the upper layer from the sea surface to either 1000 m depth or to the bottom (if the depth of the sea was less than 1000 m); some of the CTD casts (approximately every third or fourth) covered the depths from the sea surface down to the sea bottom even if the sea depth exceeded 1000 m.

To estimate the strength of the FSBW or the BSBW or both branches of the Atlantic Water, we applied standard dynamical method. The no-motion level (the zero velocity depth) was determined from the following consideration. If the baroclinic current occupies the upper layer or/and some intermediate layer, the no motion level can be chosen in a calm deep layer (where the horizontal density gradient is relatively small). On the contrary, in case of a near-bottom gravity flow, the no motion level can be reasonably chosen somewhere well above the near-bottom flow. We adopted for the no-motion level either 1000 m depth or the sea bottom depth if the latter was smaller than 1000 m for the FSBW, and some level in the vicinity of 50 m depth, where density contours were more or less flat, for the observations of BSBW in the St. Anna Trough (see also below).

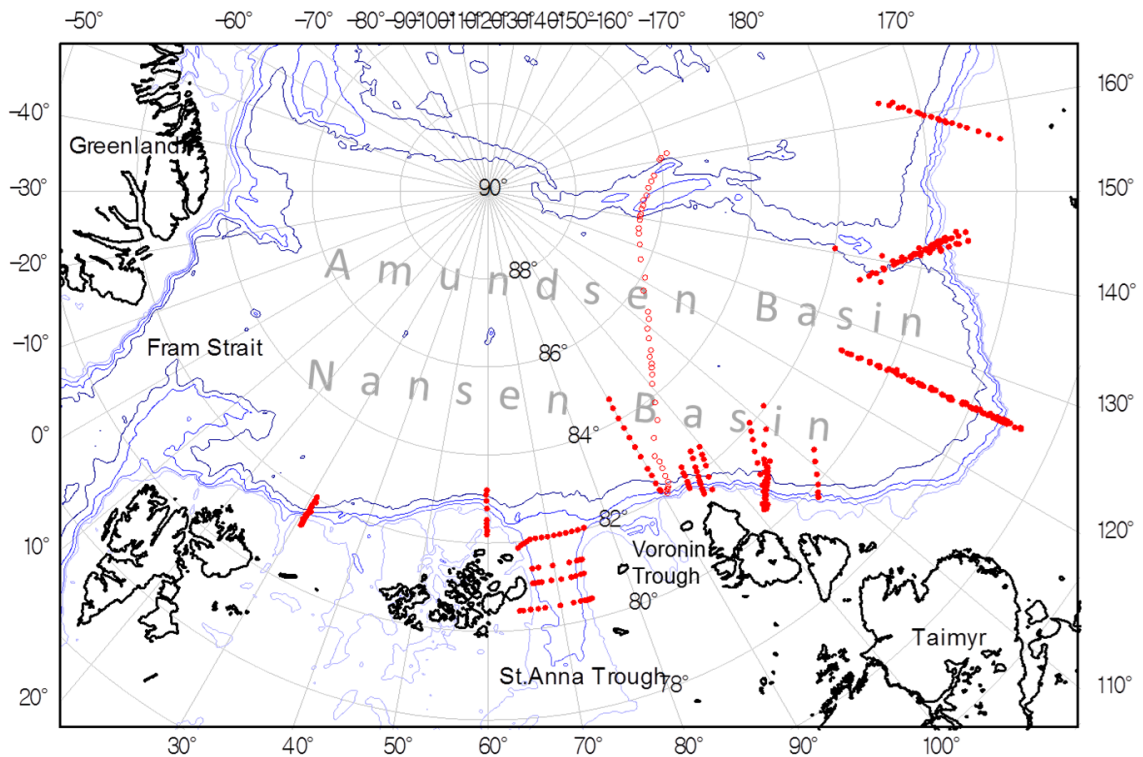


Fig. 1. Bathymetric map of the Eurasian Basin with 300, 500, 1000, and 2000 m contours shown. The red filled and blank circles are the locations of CTD stations on the NABOS and PS96 transects, respectively.

95

Since the FSBW brings saline and warm water to the Eurasian Basin, the geostrophic estimates of the volume flow rate were found by integration over the depth range with positive temperature, $\theta > 0$ °C, and relatively high salinity, $S > 34.5$ (the salinity is given in the practical salinity scale), that is, some areas in the near-surface layer with warm and fresh water (which cannot be attributed to AW) were excluded. For the observations of BSBW in the St. Anna Trough the geostrophic estimates of the volume flow rate were found by integration over a depth range with the non-averaged temperature below 0 °C and the salinity above 34.5. If both branches of AW were present on the transect, the integration was performed over the entire depth range except the cold near-surface layer ($\theta < 0$ °C) and the areas in the near-surface layer with warm ($\theta > 0$ °C) and relatively fresh ($S < 34.5$) water. The zero velocity depth in this case was chosen in accordance to the observed pattern of density contours, i.e. its resemblance with either the near-surface flow pattern or the near-bottom flow pattern (see Section 3). The details and limitation of the geostrophic velocity calculations are discussed in Zhurbas (2019).

100

105

3. Results

3.1 Variability of the thermohaline pattern on the AW pathway along the slope of Eurasian Basin

110

3.1.1 CTD transects analysis

The transformation of thermohaline signatures (i.e. patterns of salinity S , potential temperature θ , and potential density anomaly σ_θ , versus cross-slope distance and depth) of the AW flow on its pathway along the slope of the Eurasian Basin are presented in Fig.2. The σ_θ contours on transects at 31°E diverge towards the continental slope margin (to the south), shallowing above the warm/saline core of the AW and sloping down beneath it associated with an eastward subsurface flow. Such a structural feature of the distribution of isopycnic surfaces was observed on all NABOS transects taken across available continental slope at 31°E. According to Fig. 2 the warm/saline core of the Fram Strait Branch of the AW with the maximum temperature θ_{max} of 4.88°C at the depth $Z_{\theta_{max}}=102$ m and the maximum salinity S_{max} of 35.11 at the depth $Z_{S_{max}}=176$ m is found on the slope at about 1000 m isobath.

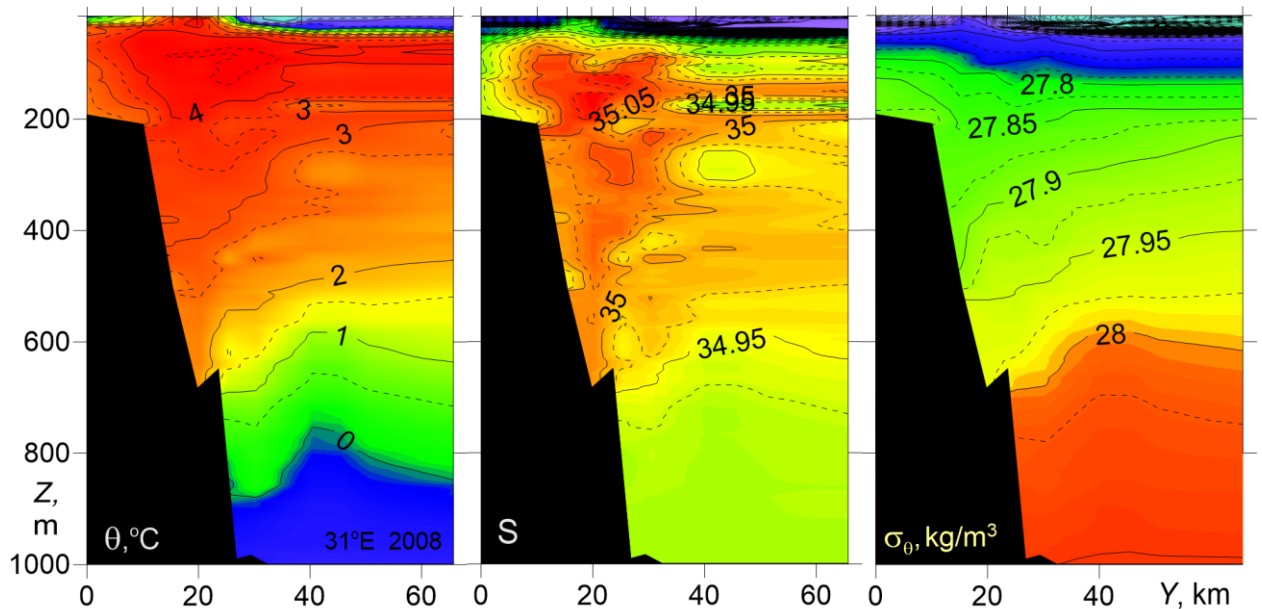


Fig. 2. Temperature θ , salinity S , and potential density anomaly σ_θ versus cross-slope distance and depth for the NABOS-2008 transect across the Eurasian Basin slope at 31°E.

Figure 3 presents temperature, salinity, and potential density versus distance and depth for two zonal transects across the St. Anna Trough at latitudes of 81 and 82°N. A stable pool of cold ($\theta < 0^\circ\text{C}$) and dense ($\sigma_\theta > 28 \text{ kg/m}^3$) water in the bottom layer is seen adjacent to the eastern slope of the trough. The transfer of the densest water pool to the eastern slope corresponds to a geostrophically balanced near-bottom gravity flow to the North. Note, that the gravity bottom currents are a typical feature of ocean dynamics and can develop in the narrows and troughs of various ocean basins (Arneborg et al., 2007; Zhurbas et al., 2012). This near-bottom gravity current carries also waters of Atlantic origin, which are strongly cooled due to mixing with shallow waters of the Arctic shelf seas (the Barents and Kara seas). Above the near-bottom

135 gravity flow of the BSBW one can observe two-core structure of warm FSBW with temperature
 up to 2.5 °C that enters the St. Anna Trough from the north-west at the western side of the trough
 and leaves it for the north-east at the eastern side of the trough. At 82°N, the BSBW overflows a
 ridge-like elevation east of the St. Anna Trough (top panels in Fig. 3). Results of studies of the
 currents ~~velocities and thermohaline characteristics of the waters masses~~ in the St. Anna Trough
 140 can be found in (Schauer et al., 2002a, b; Rudels et al., 2014; Dmitrenko et al., 2015).

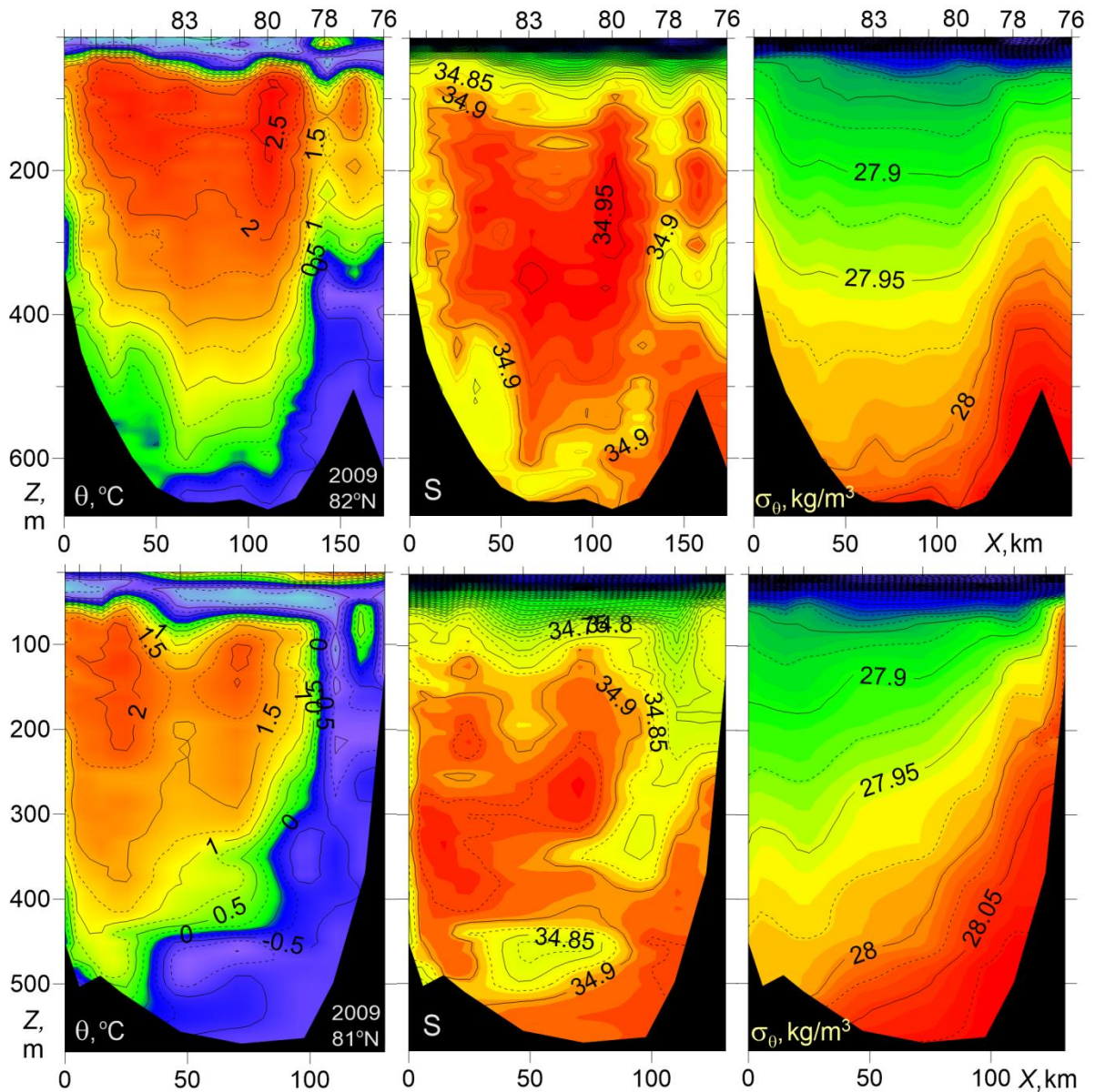


Fig. 3. Temperature θ , salinity S , and potential density anomaly σ_θ versus distance and depth for zonal transects across the St. Anna Trough at latitudes of 81°N (bottom, NABOS-2009), and 82°N (top, NABOS-2009). The X-axis is directed to the east.

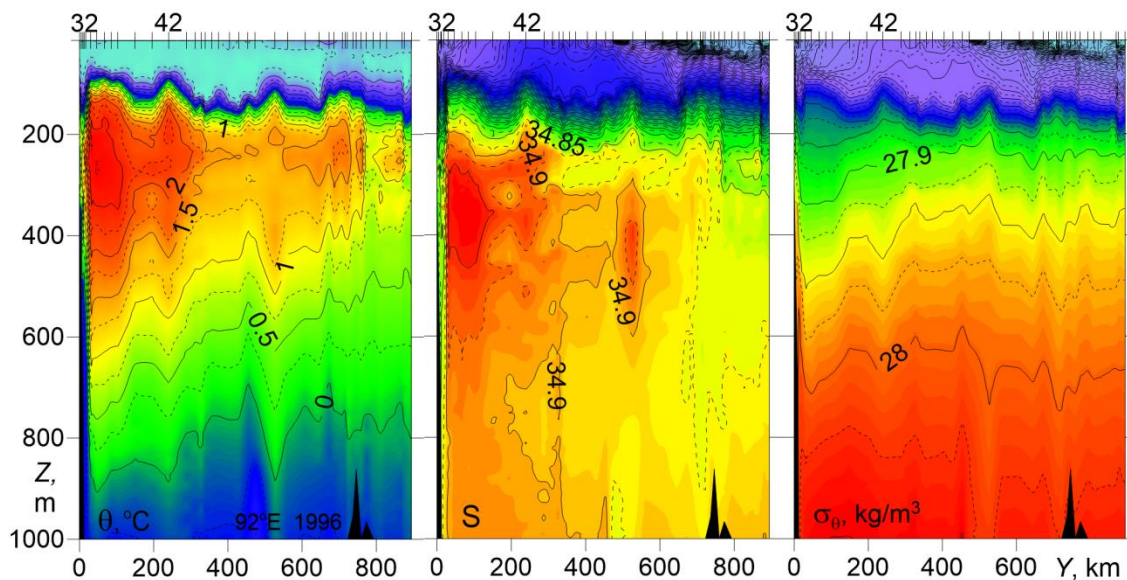
145

In order to understand the effect of the FSBW and the BSBW transformation on geostrophic volume flow rate, it is necessary to identify water masses of different origin. For that

purpose the following criterion is often used (Walsh et al., 2007; Pfirman et al., 1994): the water masses of the FSBW are characterized by $\theta > 0$ °C, and the BSBW can be identified by ~~the following expressions:~~ -2 °C $< \theta < 0$ °C, $34.75 < S < 34.95$ and $27.8 \text{ kg/m}^3 < \sigma_\theta < 28.0 \text{ kg/m}^3$. Other approaches to define BSBW are given in Schauer et al. (1997; 2002a, b) and Dmitrenko et al. (2015). According to Schauer et al. (1997; 2002a, b) the BSBW includes all waters that enter the Nansen Basin from the St. Anna and Voronin troughs. The temperature of these waters, however, can reach ~ 1 °C. The justification for this approach was based on θ - S analysis of the waters of the north-eastern part of the Barents Sea and the St. Anna and Voronin troughs. According to Dmitrenko et al. (2015), the BSBW consists of two water masses, and the temperature of the warmer water mass can only slightly exceed 0 °C (for more details see section 3.1.2). Here we will rely on the definitions of the FSBW and BSBW proposed by Dmitrenko et al. (2015).

In Fig. 4 the CTD transect at 92°E carried out in the *Polarstern*-1996 expedition just east of the entrance point of the BSBW to the Eurasian Basin from the St. Anna Trough and Voronin Trough is presented. It can be assumed that a part of the BSBW extends deep into the Basin, mixing with the FSBW, while another part of the BSBW ~~moves~~ eastward along the slope according to the general cyclonic circulation observed in the Eurasian Basin. On the presented transect the BSBW is observed in the depth range below 600 m as a narrow, about 10 km wide strip of cold water near the slope (see also Subsection 3.1.2) adjacent to a 300 km wide zone occupied by the warm FSBW. The ~~pattern of the~~ potential density of FSBW on this transect is similar to transects at 31°E. Namely, despite of the masking effect of vertical undulations of σ_θ contours caused by internal waves and mesoscale eddies (one of subsurface, intra-pycnocline eddies is probably identified at the distance of $Y=510$ km), ~~one cannot miss the tendency of shallowing/sloping down the σ_θ contours~~ above/below the FSBW core towards the continental slope margin (to the south) which, in terms of geostrophic balance implies the eastward flow of FSBW. The FSBW core on the 92°E transect is found at 40 km distance from the slope, with the maximum temperature $\theta_{max}=2.79$ °C at $Z_{\theta_{max}}=271$ m and salinity $S_{max}=34.97$ at $Z_{S_{max}}=329$ m. Therefore, the FSBW on its pathway along the slope of the Eurasian Basin from 31°E to 92°E has cooled, desalinated, sank and become denser by ~~approx.~~ 2 °C, 0.1, 150 m, and 0.1 kg/m^3 , respectively. Another ~~significant~~ feature ~~seen~~ in the PS96 transect is ~~an~~ increased temperature pool in the layer of 180–300 m at the distance of $Y=600$ – 750 km in the vicinity of the Lomonosov Ridge which can be attributed to the geostrophically-balanced FSBW return flow cyclonically circulating around the Eurasian Basin (Rudels et al., 1994; Swift et al., 1997).

According to Schauer et al. (2002b) ~~where the thermohaline structure along the PS-96 section was studied in detail~~, the horizontal and vertical scales of the BSBW were taken at 30 km and 800 m, respectively. This differs from our interpretation based on the definition of BSBW with temperature less than 0 °C.



185

Fig. 4. Temperature θ , salinity S , and potential density anomaly σ_θ versus distance and depth for cross-shelf transects at 92°E (PS-1996).

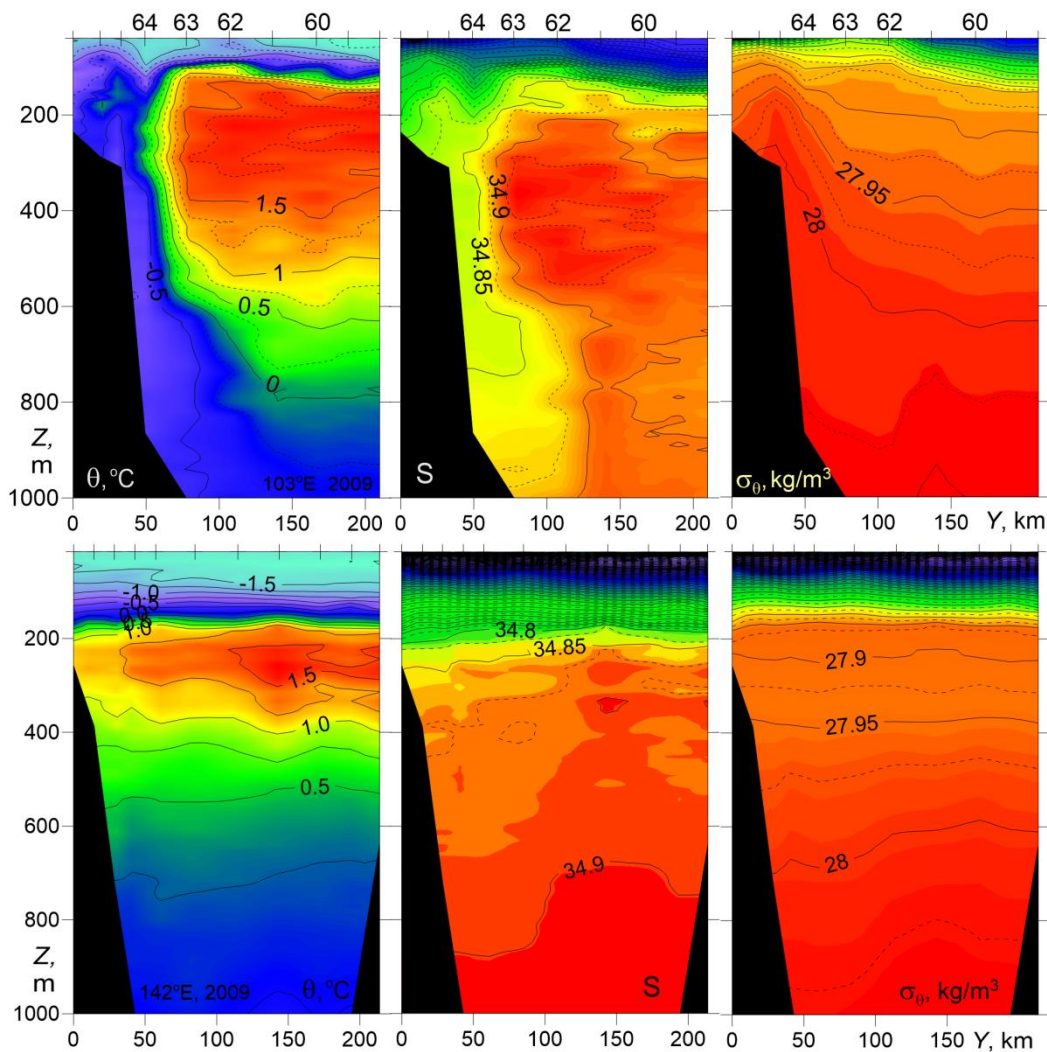
Further east, in the longitude range of 94–107 °E (NABOS-09), the denser part of BSBW ~~dives~~ under the FSBW, characterized by an eastward geostrophic current with isopycnals sloping towards the North in a 150 km wide zone adjacent to the slope (see Fig. 5, top panel). Less saline water at the slope is the less dense ~~Barents Sea Branch water~~ that has entered the Nansen Basin when the slope narrows north of Severnaya Zemlya (Schauer et al., 1997).

The vertical location of the FSBW layer ~~has not changed much relative~~ to the 92°E in the section PS-96 but the maximum temperature has further decreased: in the transect in Fig. 5, the top panel, $\theta_{max}=1.98$ °C at $Z_{\theta_{max}}=245$ m and $S_{max}=34.95$ at $Z_{S_{max}}=365$ m. The bottom panel of Fig. 5 presents the ~~data from~~ transect at 142°E (NABOS-09) which is located on the Lomonosov Ridge, between the Amundsen and Makarov Basins. The comparison of the two transects obtained in the same year shows that the vertical scale of the ~~especially~~ warm FSBW water ($\theta>1.5$ °C) has significantly decreased. Nevertheless, the FSBW waters are also observed at this longitude and affect the slopes of isopycnal surfaces in a layer up to 300 m. The cold waters with $\theta<0$ °C, which can be associated with the BSBW, are observed only at two stations in the depth range close to 1000 m, and are ~~practically~~ absent at the depths above 950 m. The isopycnal surfaces in the bottom panel of Fig. 5 are relatively flat, indicating weak geostrophic flow (see Section 3.2). ~~Note that, the water with absolutely~~ stable thermohaline stratification is well

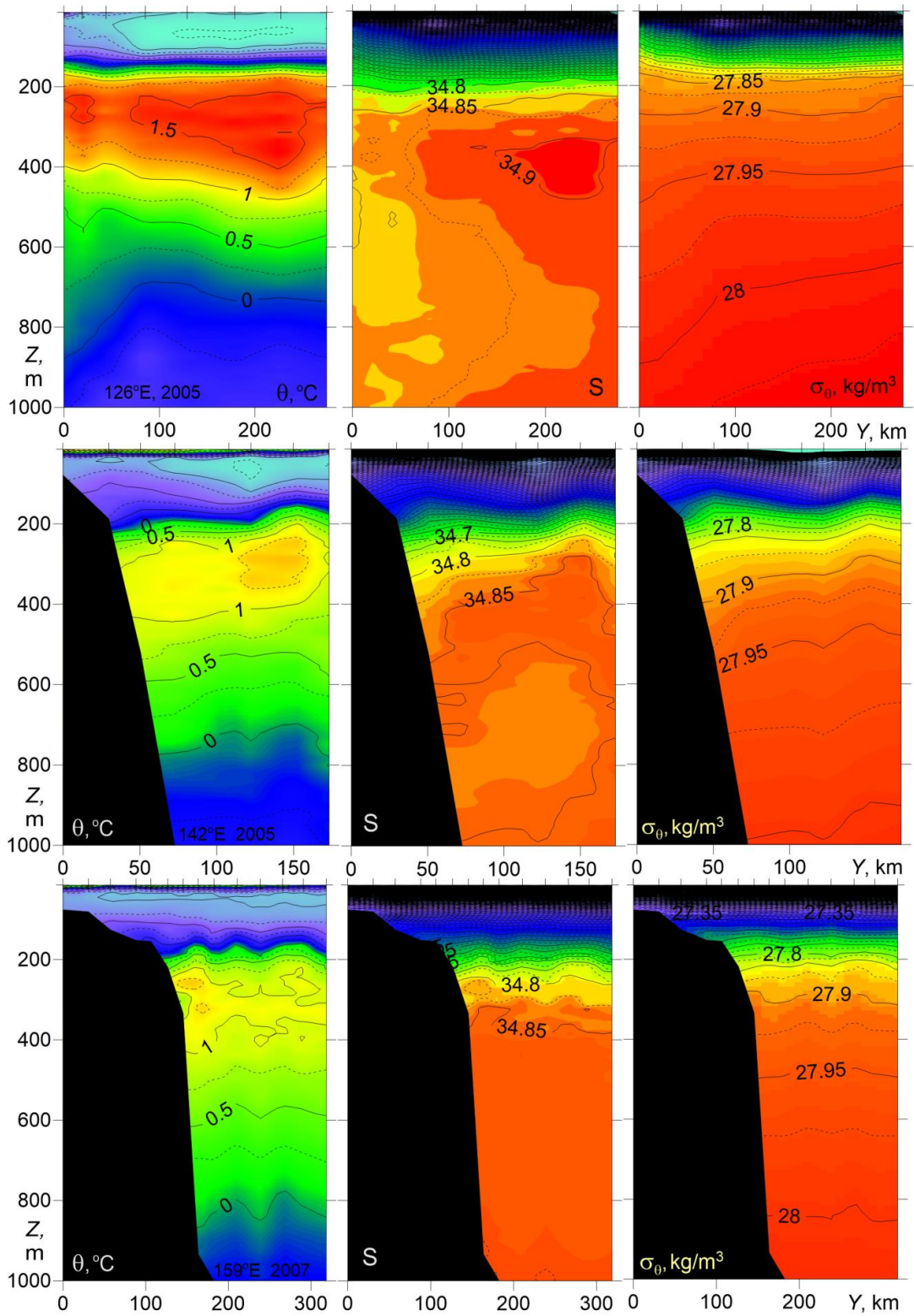
200

205 visualized (Fig. 5, bottom panel): the temperature decreases and salinity increases with depth. This feature of the mean thermohaline stratification is common to the Upper Polar Deep Water (UPDW) layer (Rudels et al., 1999).

In Fig. 6 three transects are presented, two of which were made at 126°E and 142°E (NABOS-2005) and the third one was made in the Makarov Basin at 159° E (NABOS-2007). On the transect along 126°E large slopes of isopycnic surfaces are observed, which corresponds to a fairly intensive geostrophic flow (see Section 3.2), confined to the depth range of 200–400 m, that is, to the area occupied by the FSBW. At the 142°E transect which is located on the Lomonosov Ridge, and at the 159°E transect in the Makarov Basin, the FSBW can be still identified as a warm layer within a depth range of 200–400 m, where the maximum temperature is reduced to 1.49 °C and 1.42 °C, respectively (Fig. 6). The 142°E transect implies some eastward geostrophic transport, whereas at the 159° E transect, and in the area of cold waters (the depth range below 800 m) in the sections shown in Fig. 6, the baroclinic flow is weak or absent.



220 Fig. 5. Temperature θ , salinity S , and potential density anomaly σ_θ versus distance and depth for cross-shelf transects at 103°E (upper) and 142°E (lower) (NABOS-09).



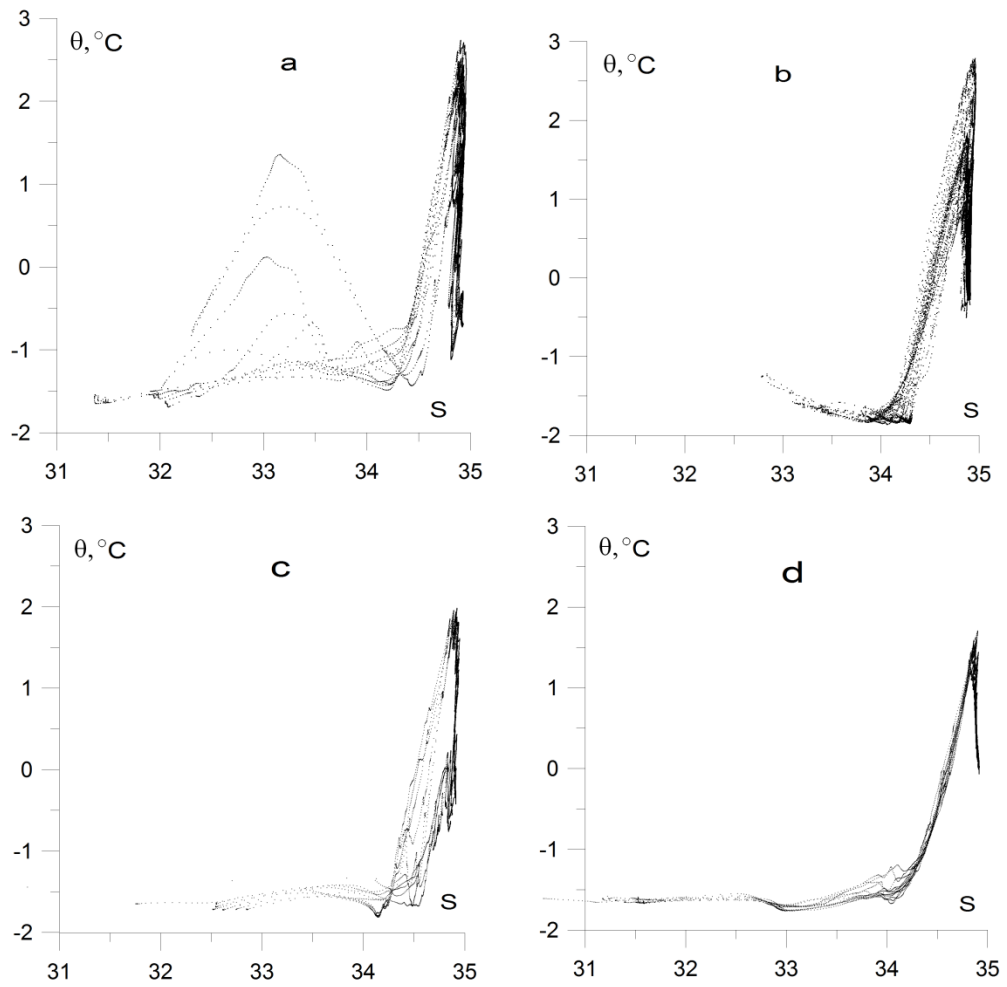
225 Fig. 6. Temperature θ , salinity S , and potential density anomaly σ_θ versus distance and depth for cross-shelf transects at 126°E, 142°E (top and middle, NABOS-2005) and 159°E (bottom, NABOS-2007).

In summary, the combined FSBW-BSBW structure with isopycnals sloping down to the north (from the slope), is typical for the longitude range 94–107°E. On the transects made along 126°E, 142°E, and 159°E, the slopes of isopycnic surfaces, indicating the baroclinic flow, were observed generally in the depth range of 200–400 m, that is in the area occupied by the FSBW. As the FSBW moved along the continental slope of the Eurasian Basin, a significant decrease of temperature was observed in the FSBW core but could be identified at all transects, including the two transects in the Makarov Basin (159°E). The cold waters on the transects along 126°E, 142°E and 159°E, which can be associated with the BSBW, had a minimum temperature above -0.5 °C, were observed in the depth range below 800 m and had a little effect on the spatial structure of isopycnic surfaces and horizontal gradient of density.

3.1.2 θ - S analysis

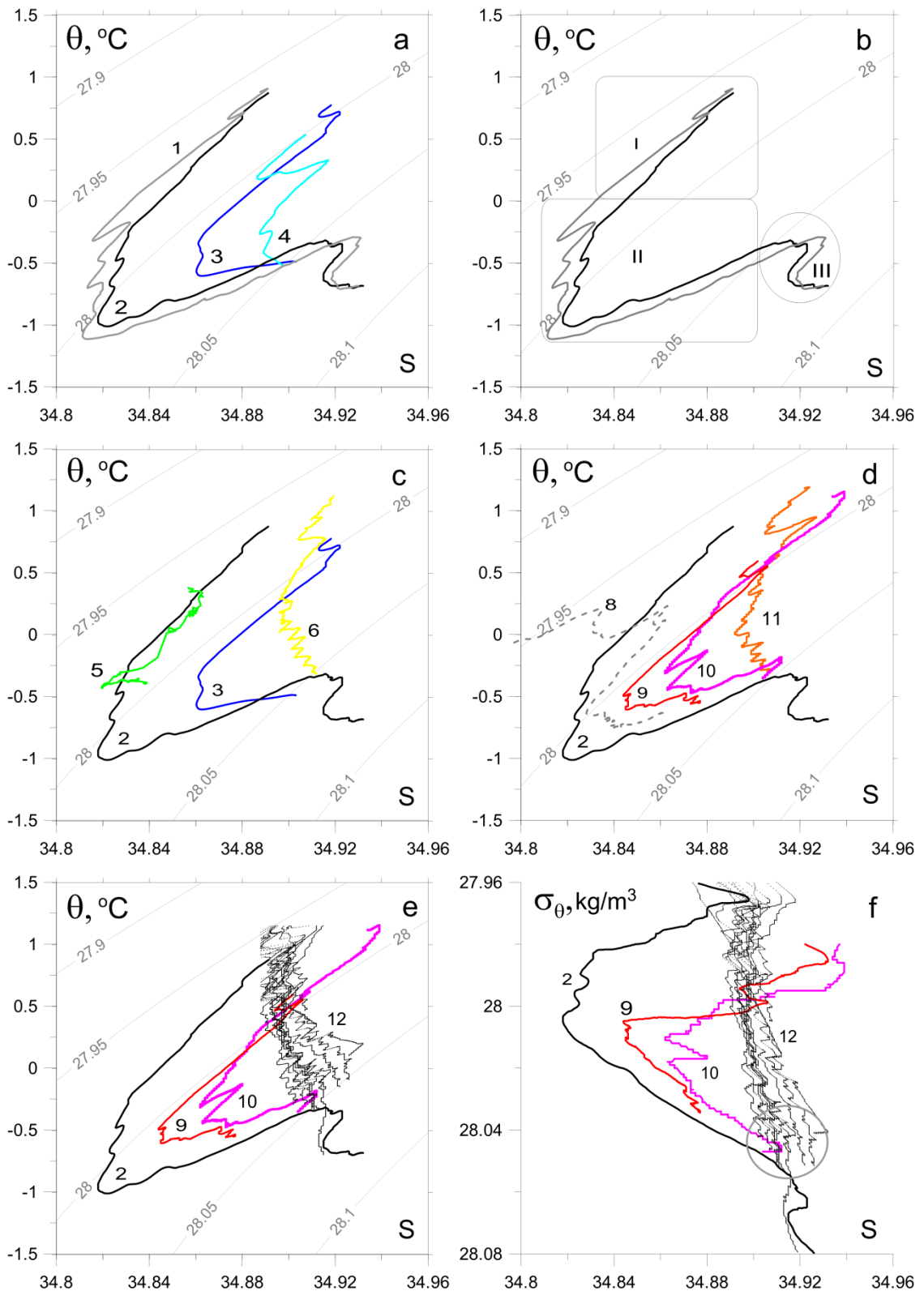
The difficulty in identifying the BSBW in the eastern part of the Nansen Basin is related to the overlapping ranges of temperature and salinity inherent to the BSBW and the UPDW: -0.5 °C $< \theta < 0$ °C, and the salinity is close to 34.9 (Rudels et al., 1994; Walsh et al., 2007). It is also important to note that the BSBW in the St. Anna Trough mixes with the FSBW. Therefore, not only the cold Atlantic Waters, which are transported by the bottom gravity current, but also mixed warmer waters can enter the Nansen Basin through the trough (see Fig. 3). A detailed θ - S analysis of different CTD sections can provide useful information on the transport and transformation of FSBW and BSBW. Note that a pronounced θ - S signal clearly indicates that the water mass has entered the area of observation. The absence of a signal indicates one of the following: a) the water mass did not enter the area of observation; b) it entered the area of observation being highly transformed, namely, mixed with other waters.

The differences in the behavior of the θ - S values are observed in the upper and deep layers of the Eurasian Basin and the St. Anna Trough (Fig.7). On the other hand, one cannot miss a similarity in the shape of the θ - S curves in the salinity range of 34.5–35.0. The similarity is obviously caused by the presence of FSBW. Fig. 7 demonstrates the transformation of the FSBW and BSBW moving along the continental slope of the Eurasian Basin. More detailed information on the BSBW transformation can be extracted from θ - S diagrams presented in Fig. 8.



255

Fig. 7. θ - S diagrams based on the CTD profiling in (a) the St. Anna Trough (NABOS-09, 82° N), (b) the PS-96 section at 92°E, and the NABOS-09 sections at 103°E (c) and 142°E (d). For convenience of presentation, the points of the θ - S curves with salinity below 30 were dropped.



260 Fig. 8. Thermohaline values of the BSBW and FSBW: a) based upon the CTD profiles, obtained
 in the St. Anna Trough (NABOS-09, section 82°N), curves 1–4 correspond to the stations (st.)
 76, 78, 83 and 80, respectively; b) the same as “a” but only curves 1 and 2 are presented; regions
 I, II, III illustrate three different water masses in accordance with (Dmitrenko et al., 2015); for
 explanation see the text; c) based upon the section of PS-96, curves 5 and 6 corresponding to st.
 265 32 and 42, respectively (depth range 600–1000 m), curves 2 and 3 are shown for the reference;

d) for CTD profiles at the 103°E section, NABOS-09, curve 8 (st. 64), curve 9 (st. 63), curve 10 (st. 62), curve 11 (st. 60), and curve 2 for the reference (see Fig. 5 for the location of the stations); e) based upon the CTD profiles in the depth range 500–1200 m measured at the 126°E (section of NABOS-09), curves 12; curves 2, 9 and 10 are shown for the reference; f) the same as “e” but presented in coordinates σ_θ, S .

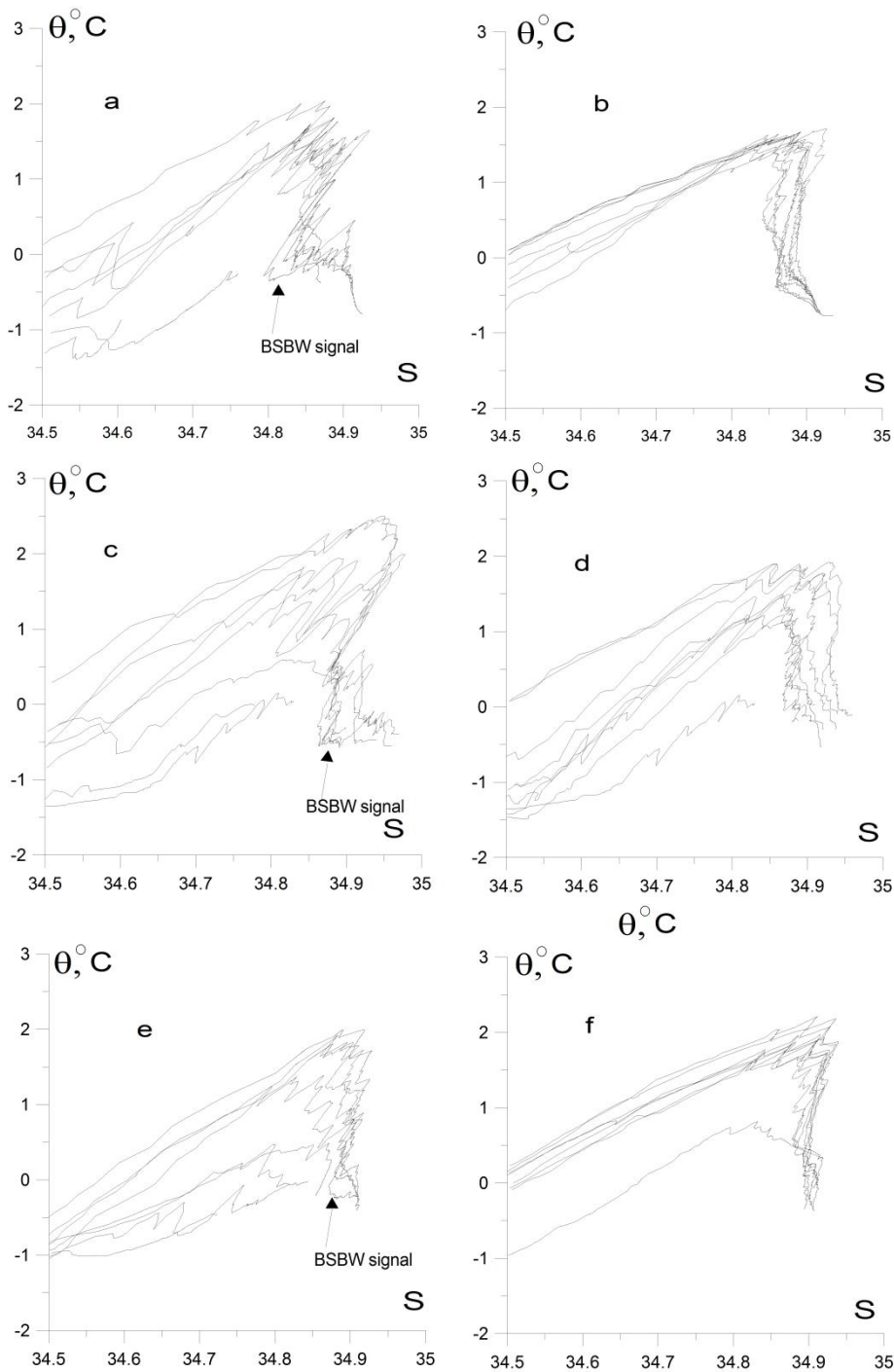
The θ - S curves marked as 1 and 2 in Fig.8a correspond to stations 76 and 78, respectively, which were located at the eastern slope of the St. Anna Trough just in the near-bottom gravity current carrying the BSBW, while the curves marked as 3 and 4 correspond to stations 83 and 80 located near the mid-point (thalweg) of the trough in the western periphery of the gravity current (the location of the stations is shown in Fig. 3). To visualize better the BSBW transformation, the points of θ - S curves in the temperature and salinity ranges of $\theta > 1.2$ °C and $S < 34.76$, respectively, were omitted. Similar θ - S curves in the St. Anna Trough were observed within NABOS Program in other years (NABOS-13, NABOS-15).

The curves 1 and 2 in Fig. 8a have similar knee-like shape (Dmitrenko et al., 2015) formed by (i) the upper warm and saline water layer of the FSBW ($\theta \gg 0$ °C), (ii) the intermediate colder and fresher water layer of BSBW ($\theta < 0$ °C) underlying the FSBW, and (iii) the denser, warmer and saltier “true” mode of the BSBW ($\theta \approx 0$ °C), see Fig. 8b: FSBW (region I), BSBW (region II), “true” mode BSBW (region III). The difference between the BSBW and “true” mode BSBW is in that the former is more diluted with the colder and fresher Barents Sea water (for more details see paper by Dmitrenko et al., 2015). We will be interested in the transformation of the main part of the knee (region II), namely the transformation of BSBW.

In Fig. 8c the comparison of typical θ - S curves related to the St. Anna Trough (they are also shown in the other panels of Fig. 8 for reference) with that of the 92°E section of PS-96 is given: the curves 5 and 6 correspond to st. 32 and st. 42 (depth range 600–1000 m) of the PS-96 section, respectively. St. 32 was located next to the slope, while st. 42 was located about 250 km apart from the slope. The coincidence of curve 5 with a part of curve 2 evidences for the BSBW moving along the slope of Nansen Basin (see Fig. 4 and its legend 1). Curve 6 corresponds to the UPDW. The θ - S diagrams for CTD profiles at the section 103°E are presented by curves 8-11 (see Fig. 5 for the locations of stations). Curves 8, 9, and 10 are similar to curve 2, and indicate the BSBW. Curve 11, being similar to curve 6 in Fig. 8c, corresponds to the θ - S values of the UPDW. However, the BSBW is not observed in the section 126°E: see Fig. 8e, where a collection of θ - S curves (collectively referred as 12) presents all CTD profiles in the depth range 500–1800 m measured at the section 126°E of NABOS-09. Also we do not observe the BSBW further to the east on the section 142°E of NABOS-09 (not shown) as well as in the Makarov Basin.

To estimate the potential density of deep waters at the sections 103°E and 126°E σ_θ - S diagrams are shown in Fig. 8f: curves 2, 9 and 10 correspond to θ - S curves 2, 9 and 10 presented in Fig. 8d, curves 12 correspond to curves 12 in Fig. 8e. As one can see, the BSBW is characterized by knee-shape diagram also in coordinates σ_θ , S . However the knee-shape diagram is not observed along 126°E in these coordinates. The dense and cold deep waters in the section 126°E have σ_θ , θ , S values typical for the “true” BSBW mode (Dmitrenko et al., 2015). Nevertheless, it is hardly correct to consider these waters (see σ_θ , S values inside the circle; Fig. 8f) as the “true” BSBW mode, since σ_θ , θ , S values of these waters satisfactorily correspond to σ_θ , θ , S values of the UPDW. To evaluate the transformation of the “true” mode of BSBW an additional analysis is required, which is beyond the scope of this paper.

The results presented in Fig. 8 show that the BSBW signal which is characterized by the knee-shape diagram in coordinates θ - S and σ_θ - S , is not visible at 126°E. This is consistent with the conclusion formulated in Subsection 3.1.1 that by 126°E the BSBW is not accompanied by any noticeable perturbations of isopycnals. Moreover, given the characteristic feature of the θ - S structure of BSBW in the St. Anna Trough (curves 1–4 in Fig. 8a) was observed in other years, we carried out a similar analysis using all available CTD data and found that the BSBW signal is either strongly weakened or not visible at this longitude (see Fig.9). The only exception was 2002, when the BSBW signal was still observed at 126°E. It suggests that the BSBW and FSBW begin to mix intensively immediately after 103°E. However, the FSBW signal is well identified at 126°E and further along the slope of the Eurasian Basin (and even in the Makarov Basin), while we cannot say the same about the BSBW signal. Thus, one may assume that east of 126°E the geostrophic volume flow rate of the AW is mainly provided by the FSBW.



325

Fig. 9. θ -S diagrams based on the CTD profiling : NABOS-05: (a) and (b), 103°E (a), 126°E (b); NABOS-06: (c) and (d), 103°E (c), 126°E (d); NABOS-08: (e) and (f), 103°E (e), 126°E (f).

3.2 Characteristics of the Atlantic Water flow and geostrophic estimates of the volume flow rate

330

The estimates of V , as well as estimates of the hydrological parameters describing the AW flow in the Eurasian and Makarov Basins, are presented in Table 1. The geostrophic estimates of the near-bottom gravity volume flow rate of the BSBW in zonal transects across the St. Anna Trough are presented in Table 2. The only exception is the transect at 82°N where the near-

bottom gravity current with a considerable eastward component due to overflow across a
335 sufficiently deep ridge (approx. 500 m deep) east of the St. Anna Trough (Fig. 3, top panels)
makes the estimate of AW transport northward questionable. Note also that ~~prior to the BSBW
entering the area of the Eurasian Basin,~~ our estimates refer to the FSBW; to east of this region
~~our estimates should be attributed to the joint contribution of two branches — the FSBW and
BSBW — to the transfer of the AW.~~

340 The hydrological parameters shown in Table 1 can be interpreted as follows. The
maximum water temperature of the AW may exceed 5 °C in cases when the AW inflow to the
Eurasian Basin consists of especially warm water masses. Typical changes in the ~~maxima
temperature and salinity~~ of the AW moving along the slope over a distance of about 1000 km are
approximately 1–2 °C and 0.1, respectively. ~~Such values of the maximum temperature of the
345 AW~~ lead to a slight increase in potential density and therefore a deviation of the AW from the
isopycnic distribution ~~should~~ be expected. ~~This effect is~~ most likely associated with the exchange
of heat, salt, and mass with the surrounding waters ~~due to the formation of~~ intrusive layering and
~~the influence of double diffusion (on the observation and study of intrusions in the Arctic Basin
see, e.g., Rudels et al., 1999; Kuzmina et al., 2011; Polyakov et al., 2012, Kuzmina et al., 2013)
350 and also with the AW core transformation by sea ice melting and cooling (Rudels, 1998).~~ The
intrusions, in particular, can also contribute to the reduction of the AW heat and salt content and
the volume flow rate. The differences in the AW heat and salt content and the volume flow rate
can be clearly seen from the PS-96 section when comparing data from stations near the
continental slope of the Eurasian Basin at 92°E and from the vicinity of the Lomonosov Ridge at
355 140°E.

It is worth noting that the maximum value of the AW temperature (θ_{max}) ~~according to the
presented data~~ is always observed in the upper layer of the Eurasian Basin ~~at the~~ depths below
the ~~density jump layer~~ but not exceeding 350 m, while the maximum salinity (S_{max}) at sections in
the eastern part of the Basin can be observed at depths greater than 1000 m.

360 $X_{\theta_{max}}$ in Table 1 is the distance of the AW core (which can be associated with θ_{max}) from
the slope/shelf boundary. The highest value and the maximum variation of this parameter is
observed near 126°E and 142°E, where ~~two-core structure of AW~~ often observed (Pnyushkov et
al., 2015).

The noticeable increase of θ_{max} in 2006 at 31°E and 103°E and the intensive warming of
365 the AW were first reported in (Polyakov et. al., 2011). The present results show that the increase
of the temperature of the AW in 2006 was also accompanied by an increase of volume transport

(see Table 1, the section along 103°E and reasonings below). This can be caused not only by the warming of the AW, but also by an increased inflow of the AW to the Eurasian Basin.

The ~~evaluations of geostrophic current~~ transport in the range of 31–159°E are characterized by a high variability (Table 1). This may be due to ~~the following reasons: a) the deviation of some sections from the normal~~ to the current; b) the difference in the horizontal scales of the sections; c) ~~some~~ uncertainty in the choice of the reference level for geostrophic calculations; d) meandering of the flow; e) the effect of synoptic quasi-geostrophic eddies on the flow volume rate. ~~All of these reasons contribute some noise to the resulting volume flow rate estimates.~~ In order to find statistically consistent estimates of the variability of geostrophic volume flow rate along the slope of the basin based on a limited ~~material~~, the following was done. The volume flow rates obtained for all sections within the range 31°–92 °E for different years were used to calculate the mean volume flow rate (region I; the number of volume flow rate values ~~to be~~ averaged is $N = 6$). Similarly, the average volume flow rate was calculated for the region 94°–107°E (region II; $N = 9$). The remaining average estimates of geostrophic volume flow rate were calculated for sections 126°E (region III; $N = 9$), 142°E (region IV; $N = 10$) and 159°E (region V; $N = 2$). Then the ~~confidence intervals with a probability of 95% (typical confidence interval)~~ and 80% (~~acceptable confidence interval for working with a limited statistical material~~) were determined using the Student t-distribution. All estimates of average volume flow rates and confidence intervals are presented in Tables 1 and 2.

~~The above mean estimates allow us to conclude that~~ the volume flow rate increases from region I to region II, then decreases to region III and ~~after that decreases to~~ region IV, followed by a sharp decrease in region V. However, ~~the 95% confidence intervals validate~~ only the difference between the volume flow rate in region II and the values in regions IV and V. Confidence intervals for regions II, IV and V are (0.46; 1.72), (0.12; 0.44) and (-0.37; 0.43), respectively. These intervals indicate that the mean volume flow rate in region II exceeds the value of the same parameter in regions IV and V with a high probability of 95%. The 80% confidence intervals overlap only for regions III and IV, (0.25; 0.53) and (0.18; 0.38), respectively. In this regard, ~~we can declare that the above described~~ change in the volume flow rate along the slope is ~~reliable~~ with a probability of 80%, except for changes in volume flow rate from region III to region IV.

The above values of the mean volume flow rate and confidence intervals also suggest that the increase in volume flow rate in 2006 ~~was caused by the climate impact~~, and not by the “noise” in the data. Indeed, the volume flow rates in regions II, III, and IV in 2006 exceeded the upper limits of the corresponding 95% confidence intervals. From statistical point of view such a

significant increase in volume flow rates at the same time in three regions is a very rare event that can hardly be explained by random “noise” in the data caused, for example, by the influence of synoptic eddies.

Let us turn our attention to the following features of the volume flow rate estimates: high
405 volume flow rate estimates at 96°E, 103°E, 107°E, a negative volume flow rate estimate at
126°E in 2013 and low volume flow rate estimates at 31°E, 98°E in 2009 (Table 1). Indeed, the
AW volume flow rate in the BSBW area of entry into the Eurasian Basin in 2013 was almost
equal to the maximum volume flow rate in 2006 (103°E) and was quite high up to the longitude
107°E. This phenomenon as well as the intense warming in 2006 can be associated with the
410 ~~impact of climate conditions. The~~ negative volume flow rate at 126°E was, ~~according to the~~
~~authors, due to~~ the influence of local return flows which can be observed near the slope
(Pnyushkov et al., 2015). Low FSBW volume flow rate estimates in 2009 are probably
associated with a strong deviation of the flow from the slope, which ~~may have been resulted in~~
~~an underestimation of~~ the AW volume flow rates, due to the small length of the cuts to the north
415 (see also below). Another reason may be a sharp decrease ~~the intensity of the flow of the AW~~
~~through the Fram Strait that most likely took place that year.~~

~~It is important to analyze average values of volume flow rate V_{mean} in region I and in the St.~~
~~Anna Trough.~~ The mean value of the FSBW volume flow rate is $V_{mean} = 0.5$ Sv. This estimate of
volume flow rate is about half the estimate of the BSBW mean volume flow rate, $V_{mean} = 0.79$ Sv
420 ($N = 3$, Table 2). ~~(The 80% confidence intervals do not overlap indicating that the BSBW~~
~~volume flow rate does exceed the FSBW volume flow rate).~~ The BSBW mean volume flow rate
exceeding nearly twice the FSBW mean volume flow rate results in a dominance of the BSBW
pattern of potential density contours in the longitude range of 94–107°E (region II), where both
branches of the AW are present. Moreover, the sum of the mean values of the FSBW and the
425 BSBW volume flow rate geostrophic estimates, $V_{mean} = 0.5 + 0.79 = 1.29$ Sv, corresponds well to
~~the mean geostrophic estimate of volume flow rate for~~ the combined FSBW and BSBW flow
within the region II: $V_{mean} = 1.09$ Sv. Thus, the increase in geostrophic volume flow rate in region
II is mainly due to the influence of the BSBW. ~~It should be noted that, according to sections~~
~~3.1.1 and 3.1.2,~~ the decrease in geostrophic volume flow rate in region III can also be associated
430 primarily with the BSBW, namely, with the decrease in the BSBW signal in 126°E section and
further along the slope.

Finally, at the ~~section 159°E located~~ in the Makarov Basin, the geostrophic estimate of the along-slope volume flow rate of mixed waters of the FSBW and the BSBW has further greatly reduced down to $V_{mean} = 0.03$ Sv ($N = 2$), which is of more than one order of magnitude smaller than that in the Nansen and Amundsen Basins. Despite the low statistical significance of the latter estimate (due to small value of $N = 2$) one may conclude that the major part of the AW entering the Arctic Ocean circulates cyclonically within the Nansen and Amundsen Basins, and only its small part flows to the Makarov Basin (Rudels et al., 2015; Rudels, 2015). However, additional studies ~~using more CTD data~~ are required to confirm this result.

440 Table 1. Characteristics of the Atlantic Water flow in the course of its propagation along continental slope of the Eurasian Basin of the Arctic Ocean. *Dist* is the along-slope distance from the Fram Strait; θ_{max} is the maximum temperature; $\sigma_{\theta}(Z_{\theta_{max}})$, $S(Z_{\theta_{max}})$, $Z_{\theta_{max}}$, and $X_{\theta_{max}}$ are the values of potential density, salinity, depth, and lateral displacement from the slope for the point θ_{max} ; S_{max} and $Z_{S_{max}}$ are the ~~same as θ_{max} and $Z_{\theta_{max}}$ but for the salinity~~; V is the geostrophic estimate of the volume flow rate. The mean values and 95% / 80% confidence intervals of the volume rate, V_{mean} , calculated separately for CTD transects at 31–92°E, 94–107°E, 126°E, 142°E and 159°E, are ~~presented too~~. The last row in the Table presents the characteristics of the return flow of the AW by the Lomonosov Rigde at the longitude 140°E and latitude 86.5°N (PS96, see Fig. 1). Year is given in the first column (e.g. NABOS06 corresponds to 2006).

<i>Exp</i>	<i>Lon</i> [°E]	<i>Dist</i> [km]	θ_{max} [°C]	$\sigma_{\theta}(Z_{\theta_{max}})$ [kg/m ³]	$S(Z_{\theta_{max}})$	$Z_{\theta_{max}}$ [m]	$X_{\theta_{max}}$ [km]	S_{max}	$Z_{S_{max}}$ [m]	V [Sv]
NABOS06	31	404	5.670	27.579	34.980	42	-11	35.099	72	0.57
NABOS08	31	404	4.883	27.771	35.103	101	0	35.105	176	0.80
NABOS09	31	404	3.691	27.818	34.999	89	0	35.002	91	0.10
NABOS09	60	856	2.503	27.891	34.951	175	10	34.981	363	0.47
NABOS13	90	1290	2.600	27.903	34.975	250	41	34.996	333	0.46
PS96	92	1322	2.786	27.875	34.960	271	33	34.968	329	0.58
$V_{mean} = 0.50 \pm 0.24 / \pm 0.14$ Sv										
NABOS15	94	1355	2.445	27.946	35.012	331	33	35.015	365	0.47
NABOS13	96	1388	2.548	27.902	34.969	207	70	34.978	264	2.06
NABOS09	98	1421	2.300	27.906	34.948	220	79	34.971	345	0.09
NABOS05	103	1561	2.029	27.870	34.876	179	39	34.934	309	0.32
NABOS06	103	1561	2.528	27.888	34.950	220	50	34.978	260	2.23
NABOS08	103	1561	1.980	27.886	34.891	201	60	34.929	325	0.42
NABOS09	103	1561	1.984	27.913	34.925	244	50	34.951	365	0.87
NABOS13	103	1561	2.278	27.904	34.942	215	80	34.956	419	1.59
NABOS13	107	1695	1.903	27.937	34.945	359	120	34.948	404	1.77
$V_{mean} = 1.09 \pm 0.63 / \pm 0.38$ Sv										
NABOS02	126	2104	1.406	27.938	34.902	324	243	34.932	2061	0.05
NABOS03	126	2102	1.341	27.941	34.899	336	342	34.921	1886	0.41
NABOS04	126	2102	1.770	27.906	34.896	271	87	34.925	2431	0.61
NABOS05	126	2102	1.695	27.936	34.926	359	227	34.935	2841	0.75
NABOS06	126	2102	1.905	27.923	34.930	284	193	34.960	968	0.77
NABOS07	126	2102	2.085	27.907	34.928	266	242	34.942	340	0.60
NABOS08	126	2102	2.195	27.885	34.911	206	235	34.939	365	0.31
NABOS09	126	2102	1.907	27.909	34.913	316	33	34.932	1018	0.40
NABOS13	126	2102	1.946	27.937	34.949	346	228	34.951	428	-0.21

NABOS15	126	2102	1.653	27.918	34.898	246	400	34.942	3816	0.22
$V_{mean} = 0.39 \pm 0.22 / \pm 0.14$ Sv										
NABOS03	142	2456	1.089	27.912	34.841	269	41	34.862	1000	0.06
NABOS04	142	2456	1.401	27.909	34.865	281	0	34.907	1608	0.21
NABOS05	142	2456	1.492	27.906	34.870	284	100	34.906	1550	0.26
NABOS06	142	2456	1.981	27.874	34.876	234	111	34.960	1016	0.60
NABOS07	142	2456	1.855	27.879	34.870	231	0	34.920	2064	0.09
NABOS08	142	2456	1.599	27.915	34.890	260	200	34.908	347	0.23
NABOS09	142	2456	1.704	27.915	34.900	253	101	34.917	1082	0.22
NABOS13	142	2456	1.475	27.940	34.909	331	115	34.926	1150	0.18
NABOS15	142	2456	1.353	27.936	34.892	326	106	34.913	1372	0.63
$V_{mean} = 0.28 \pm 0.16 / \pm 0.10$ Sv										
NABOS07	159	2783	1.424	27.887	34.839	255	0	34.880	1075	-0.01
NABOS08	159	2783	1.383	27.893	34.843	245	0	34.889	1266	0.06
$V_{mean} = 0.03 \pm 0.40 / \pm 0.10$ Sv										
PS96back	140E 86.5N	3178	1.812	27.890	34.880	219	≈ 700	34.902	472	-0.09

450

Table 2. Geostrophic estimates of the volume flow rate for near-bottom gravity flow of the Barents Sea Branch of Atlantic Water (BSBW) on zonal transects across the St. Anna Trough.

<i>Exp</i>	NABOS09	NABOS13	NABOS15	
<i>Lat</i> [°N]	81.00	81.33	81.41	V_{mean}
<i>V</i> [Sv]	0.89	0.73	0.76	$0.79 \pm 0.22 / \pm 0.10$

455 3.3 Interannual variability of the AW temperature-salinity values and the volume flow rate

Within the NABOS project, ~~in accordance with Table 1,~~ the cross-slope CTD transects at 103°E, 126°E, and 142°E were repeatedly performed for a number of annual campaigns: 2005, 2006, 2008 and 2013 (103°E), 2002–2009, 2013 and 2015 (126°E), 2003–2009, 2013, and 2015 (142°E). ~~The repeated transects may contain some information on~~ inter-annual variability of the AW, ~~and we attempted to explore such a possibility.~~

Time series of the ~~maximum temperature of the AW,~~ θ_{max} , and the related values of salinity $S(\theta_{max})$ and potential density anomaly $\sigma_{\theta}(\theta_{max})$ (Fig. 10) show that the period of 2006–2008 was characterized by ~~not only~~ an increased temperature of the AW in the eastern part of the Eurasian Basin, ~~but~~ an increased salinity and density reduction. The temperature excess during this period was as large as 0.6–1.0 °C relative to 2002–2003 and 0.3–0.6 °C relative to 2013–2015. ~~The time series of corresponding values of salinity~~ $S(\theta_{max})$ displayed in 2006 local maxima at the transects 126°E and 142°E, and the absolute maximum at the transect 103°E; the salinity excess for the maxima largely decreased with the longitude from approximately 0.06 at 103°E to less than 0.01 at 142°E. ~~In accordance with our analysis the time series of~~ θ_{max} had a maximum in 2013 but only at 103°E (see Table 1 and Fig.10). The time series of $S(\theta_{max})$ display an increase of AW salinity in 2006–2008 and 2013 also, that can be referred to as a AW salinization in early

470

2000s. The ~~change of salinity of AW at 142°E in time also draws attention to the following aspect: the salinity~~ increases almost monotonously in the period from 2003 to 2013. ~~How can such behavior of salinity be explained~~ is not clear. It is also worth noting that the maxima of θ_{max} and $S(\theta_{max})$ in 2006 and 2013 (at 103°E) were accompanied by ~~the volume flow rate highs~~.

4 Discussion

Here we discuss the following issues: a) differences in the identification of the BSBW; b) a comparison of the geostrophic volume flow rate estimates with other studies; c) the weakening of the BSBW signal at 126 °E and further east.

a) Advection and interaction of waters with different θ - S characteristics in the Arctic Basin, as well as the impact of climate change that has been observed over the past decade (Polyakov et al., 2017) complicate an accurate identification of water masses. However, a robust approach ~~to the determination of the FSBW and BSBW, which was~~ proposed in Dmitrenko et al. (2015), is effective for distinguishing the water masses of ~~these AW~~ branches. As an exception, this approach ~~does not take into account some cases, namely~~ when the FSBW temperature is below 0 °C (see Fig. 2 in Dmitrenko et al., 2015), and/or the BSBW temperature is close to 1 °C (see Fig. 6 in Schauer et al., 2002a). If such cases are rare, then either of the two approaches can be used to identify the BSBW and FSBW. Indeed, the identification of the BSBW on the PS-96 section in our case (we used the approach proposed by Dmitrenko et al., 2015; see paragraph 3.1.1) does not differ much from that proposed by Schauer et al. (2002b). However, these discrepancies can lead to almost an order of magnitude difference in estimates of the volume flow rate of the BSBW only due to the differences in the BSBW cross-sectional area.

b) Based on the velocity measurements with moored instruments (1997–2010) in the area of the West Spitsbergen Current (WSC) near ~~the~~ Fram Strait (zonal transect at ~78°50' N), ~~it was found that~~ approximately 3 Sv of the AW flow into the Nansen Basin (Beszczynska-Möller et al., 2012). The long-term mean volume transport confined to the WSC core branch (or Svalbard branch in accordance with Schauer et al., 2004) included 1.3 ± 0.1 Sv of the AW warmer than 2°C. The offshore WSC branch (or Yermak branch) carried on average 1.7 ± 0.1 Sv of the AW. ~~Investigation of water transport in and north of the Fram Strait based upon CTD measurements on zonal and meridional sections have been done by Marnela et al. (2013).~~ The variability range of ~~the estimates of~~ the AW geostrophic transport of the Svalbard branch ~~was calculated~~ for meridional sections ~~made in~~ 1997, 2001, and 2003 (summer/fall), ~~and~~ was between 0.06 Sv and 0.7 Sv. In Kolås and Fer (2018) observations of the oceanic current and thermohaline field (in summer 2015) in the three sections were used to characterize the evolution of the WSC along

505 170 km downstream distance. Geostrophic transports were calculated on the basis of absolute geostrophic velocities and it was shown that from 0.6 Sv to 1.3 Sv of the AW is carried by the Svalbard branch. In accordance with earlier studies of the currents in the Fram Strait, recirculation of the AW can be significant, and the volume flow rate of the AW entering the Arctic Ocean can be equal only 1 Sv (Rudels, 1987), or it ranges from 0.6 Sv to 1.5 Sv (Aagaard and Carmack, 1989).

Our estimate of the mean volume flow rate V_{mean} in region I (31°–92 °E) is in the range of variation in the above estimates. However, the upper confidence limit of our estimate does not reach 1 Sv. Moreover, we used the inequality $T > 0^{\circ}\text{C}$ to identify the AW while in Beszczynska-Möller et al. (2012) the volume flow rates of the AW entering the Eurasian Basin through the Fram Strait were determined from the $T > 2^{\circ}\text{C}$ condition. In this regard, we can admit that our assessment is somewhat underestimated. Probably, this may be due to the fact that the sections along the longitudes 31°E (see Fig. 1) are less than 100 km. Actually, at the sections along this longitude (Fig. 2, upper panel) only a part of the FSBW is observed. Given that the volume flow rate estimate is sensitive to the accepted value of cross-sectional area of the AW (see issue “a” above), the volume transport may be underestimated. One cannot also ignore the fact that horizontal density gradients of the geostrophic flow can be strengthened or weakened during the formation and passage of synoptic eddies, the influence of which on the average density field cannot be filtered out. According to Perez-Hernandez et al. (2017) north of Svalbard (between 21 and 33°E) in September, 2013, a large difference was found in the estimates of geostrophic volume flow rate (from 0.53 Sv to 3.39 Sv) due to the passage of eddies and meandering of the current. Våge et al. (2016) based on geostrophic velocities at two CTD sections across the boundary current near 30° E (September, 2012) evaluated a net AW volume flow rate of 1.6 ± 0.3 Sv. Authors of this paper found evidence of a large eddy affecting the mean volume transport calculations. The barotropic velocity component, which is not taken into account in our estimates, can also affect the values of the volume flow rates. However, if the ice cover in the Eurasian Basin is high, the barotropic addition to the flow velocity in a stratified ocean hardly can play a decisive role. In accordance to cruise reports, the NABOS CTD sections were characterized by the ice concentration of 50–100% (see <https://uaf-iarc.org/nabos-cruises/>). Exceptions occurred in the near-slope areas of the Laptev Sea, that is, in the sections along $\sim 126^{\circ}\text{E}$, where the ice concentration varied from 0 to 100%, having a maximum value in the northern part of the sections. In such areas, the contribution of the barotropic component to the flow velocity can be very significant. For example, using long-term measurements (1995 – 1996) from a mooring in the near-slope area of the Laptev Sea, Woodgate et al. (2001) showed that the contribution of the

540 barotropic component to the velocity of the Arctic Ocean Boundary Current (AOBC) was equal to the contribution of the first three baroclinic modes. ~~To estimate the volume flow rate they assumed that the~~ average velocity based on the measurements in the upper 1200 m layer was 4.5 cm/s and ~~the horizontal extension of the flow was 50–84 km. At such values of the velocity and cross section of the flow~~ the volume flow rate was estimated at 5 ± 1 Sv. This ~~estimate differs from~~ our average estimate of the AW volume flow rate along 126 °E (0.39 ± 0.22 , Table 1) by an 545 order of magnitude. Such a difference can be explained not only by the absence of a barotropic contribution in our case, but also by the fact that we took into account the volume transport of AW only (i.e. the cold, low-salinity surface layer was excluded) and considered certain season (August and September). Indeed, according to long-term measurements at 6 moorings on a section along 126 °E, the AOBC volume flow rate varied from 0.3 Sv to 9 Sv (Pnyushkov et al., 550 2018 b). Such a wide range in volume flow rate estimates is probably due to a combined effect of seasonal variability and mesoscale eddies (Pnyushkov et al., 2018 a).

The fact that seasonal variations can in some cases significantly affect the AW volume flow rates (see also the discussion of ~~different estimates of the AW volume flow rate in~~ Pnyushkov et al., 2018 b) is confirmed by a number of observations (Schauer et al., 2002a; 555 Beszczynska-Möller et al., 2012; Pnyushkov et al., 2018 b). For example, the volume flow rate of the AW in the northwestern part of the Barents Sea was 0.6 Sv ~~according to velocity measurements in summer~~ (Schauer et al., 2002a). This ~~estimate~~ agrees well with our estimate of the transport of AW in the St. Anna Trough, 0.79 ± 0.22 Sv (Table 2). However, the analysis of current velocity measurements in the winter season at the same section in the northwestern part 560 of the Barents Sea ~~gives a~~ completely different estimate of ~ 2.6 Sv (Schauer et al., 2002a).

c) According to Dmitrenko et al. (2009), the BSBW ~~signal is~~ satisfactorily identified at 142°E. However, a “pattern” in the θ - S diagram far from the place of the BSBW entry into the Eurasian Basin can be regarded as the BSBW signal, if it maintains the similarity with the “pattern” of the BSBW at the exit from the St. Anna Trough, that is, with the so-called “knee” 565 (Dmitrenko et al., 2015). Our analysis showed that the “knee” is regularly observed at 103°E, while at 126°E it is ~~either absent or weakens strongly and~~ distorted. ~~Apparently this is quite natural,~~ since the flow velocity is small, and the BSBW covers a distance from 103°E to 126°E for 1–2 years. However, despite of such a long travel time, Fram Strait branch is well identified not only at 126°E, but also further along the slope. ~~It seems acceptable to associate this situation~~ 570 ~~with characteristic features of~~ transformation and mixing of, primarily, the BSBW. The BSBW transformation can be due to various reasons, including mixing with the FSBW caused by thermohaline intrusive layering ~~at absolutely stable stratification~~ (Merryfield, 2002; Kuzmina et al., 2013; Kuzmina et al., 2014; Kuzmina, 2016, Zhurbas N., 2018; Kuzmina et al., 2018, 2019).

Indeed, the intrusive layering in the ocean influences the processes of exchange and mixing of various water masses (see, e.g., Stern, 1967; Fedorov, 1976; Joyce, 1980; Zhurbas et al., 1993; Rudels et al., 1999; Kuzmina, 2000; Walsh and Carmack, 2003). Other reasons for the BSBW signal disappearance may be: the influence of the slope topography, the impact of local counterflows near the slope (see, for example, Pnyushkov et al., 2015), lateral convection (Ivanov and Shapiro, 2005; Ivanov and Golovin, 2007; Walsh et al., 2007), the impact of the Arctic Shelf Break Water (Aksenov et al., 2011; Ivanov and Aksenov, 2013) and mixing due to eddies (Schauer et al., 2002; Dmitrenko et al., 2008; Aagaard et al., 2012; Pnyushkov et al., 2018a). The understanding of the processes of transformation and mixing of the BSBW and FSBW is necessary to verify an important concept proposed by Rudels, et al. (2015) that the BSBW supplies the major part of the AW to the Amundsen, Makarov and Canadian Basins, while the FSBW remains almost fully in the Nansen Basin.

5 Summary

The θ - S properties and the volume flow rate estimates of the current carrying the AW in the Eurasian Basin and St. Anna Trough were obtained based on the analysis of CTD data collected within the NABOS program in 2002–2015; additionally CTD transect PS-96 was considered. All estimates are given in tabular form.

FSBW was present at all transects, including the two transects in the Makarov Basin (159°E), while the cold waters at the transects along longitudes 126°E, 142°E and 159°E, which can be associated with the influence of the BSBW, were observed in the depth range below 800 m and had little effect on the spatial structure of isopycnic surfaces and horizontal gradient of density. It is shown using θ - S analysis that the BSBW signal, which is characterized by the knee-shape feature in coordinates θ , S and σ_θ , S (see Fig.8), is either strongly weakened or not visible at the longitude 126°E (excluding the observations in 2002 at 126 °E), while the FSBW signal is well identified at 126°E and further along the slope of the Eurasian Basin. Based on the revealed features of the temperature, salinity and density fields, it is suggested that east of 126°E the geostrophic volume transport of AW is mainly provided by the FSBW.

In order to assess spatial variability of the AW geostrophic volume flow rate, standard statistical analysis was used. It is shown with a 80% probability that the geostrophic volume flow rate increases from the region of 31°E–92°E (0.5 ± 0.14 Sv) to the region of 94°E–107°E (1.09 ± 0.38 Sv), then decreases to the region of 126°E (0.39 ± 0.14 Sv) and becomes small (0.03 ± 0.1 Sv) in the Makarov Basin (159°E).

The temporal variability of hydrological parameters and of the AW volume flow rate is summarized as follows. The time series of θ_{max} had an absolute maximum in 2006–2008 that can be interpreted as a result of heat pulse in the early 2000s (Polyakov et al., 2011). In accordance with our analysis the time series of θ_{max} had a maximum in 2013 but only at the longitude 103°E (Table 1 and Fig.10). The time series of $S(\theta_{max})$ also display an increase of AW salinity in 2006–2008 and 2013, that can be referred to as a AW salinization in the early 2000s. Moreover the salinity increases almost monotonously in the period from 2003 to 2013 at 142°E . It is important to underline also that the maxima of θ_{max} and $S(\theta_{max})$ in 2006 and 2013 (103°E) are accompanied by the volume flow rate highs. A significant increase in geostrophic volume flow rate identified in 2006 is shown to be caused by climate impact.

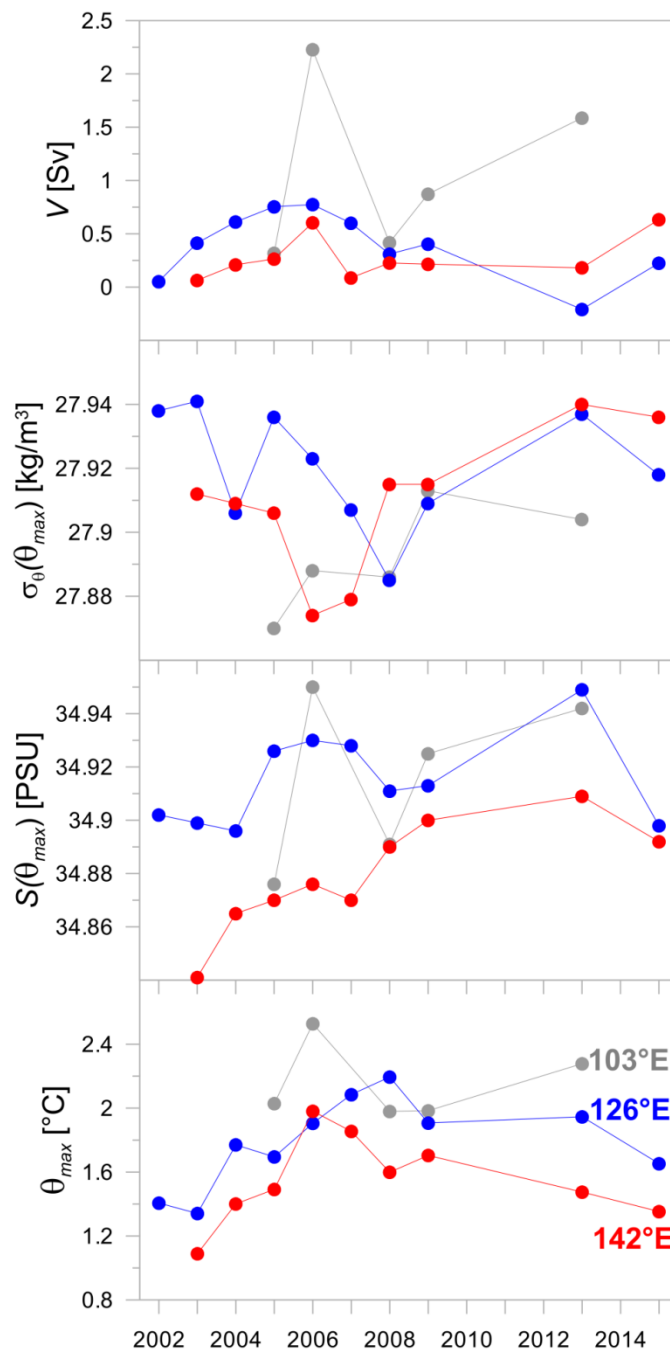


Fig. 10. Interannual variability of the maximum temperature θ_{max} and the related values of salinity $S(\theta_{max})$, potential density anomaly $\sigma_{\theta}(\theta_{max})$ and volume flow rate V on the cross-slope transects at 103°E, 126°E and 142°E.

- 620 *Acknowledgments.* This research, including the approach development, data processing and interpretation, performed by Nataliya Zhurbas, was funded by Russian Science Foundation, project no. 17-77-10080. Natalia Kuzmina (θ - S analysis, statistical analysis, participation in discussion) was supported by the state assignment of the Shirshov Institute of Oceanology RAS (theme no. 0149-2019-0003).
- 625 The authors are very grateful to the NABOS group for providing the opportunity to use the CTD-data.
- The authors are very grateful to the editor for evaluating the article and help in the work on the text and anonymous reviewers for useful comments.

References

- 630 Aagaard, K.: On the deep circulation of the Arctic Ocean, *Deep-Sea Res.*, 28, 251–268, 1981.
- Aagaard, K., and Carmack, E. C.: The role of sea ice and other fresh water in the Arctic circulation, *J. Geophys. Res.*, 94(C10), 14485–14498, doi: 10.1029/JC094iC10p14485, 1989.
- Aagaard, K., Andersen, R., Swift, J., and Johnson, J.: A large eddy in the central Arctic Ocean, *Geophys. Res. Lett.*, 35, L09601, doi: 10.1029/2008GL033461, 2008.
- 635 Aksenov, Y., Ivanov, V. V., Nurser, A. J. G., Bacon, S., Polyakov, I. V., Coward, A. C., Naveira-Garabato, A. C., and Beszczynska-Moeller, A.: The Arctic Circumpolar Boundary Current, *J. Geophys. Res.*, 116, C09017, 1–28, doi:10.1029/2010JC006637, 2011.
- Arneborg, L., Fiekas, V., Umlauf, L., and Burchard, H.: Gravity current dynamics and entrainment – A process study based on observations in the Arkona Basin, *J. Phys. Oceanogr.*,
- 640 37, 2094–2113, doi:10.1175/JPO3110.1, 2007.
- Beszczynska-Möller, A., Fahrbach, E., Schauer, U., and Hansen, E.: Variability in Atlantic water temperature and transport at the entrance to the Arctic Ocean, 1997–2010, *ICES Journal of Marine Science*, 69(5), 852–863, doi: 10.1093/icesjms/fss056, 2012.
- Dmitrenko, I. A., Kirillov, S. A., Ivanov, V. I., and Woodgate, R.: Mesoscale Atlantic water
- 645 eddy off the Laptev Sea continental slope carries the signature of upstream interaction, *J. Geophys. Res.*, 113, C07005, doi: 10.1029/2007JC004491, 2008.
- Dmitrenko, I. A., Kirillov, S. A., Ivanov, V. V., Woodgate, R. A., Polyakov, I. V., Koldunov, N., Fortier, L., Lalande, C., Kaleschke, L., Bauch, D., Hölemann, J. A., and Timokhov, L. A.: Seasonal modification of the Arctic Ocean intermediate water layer off the eastern Laptev
- 650 Sea continental shelf break, *J. Geophys. Res.-Oceans*, 114, C06010, <https://doi.org/10.1029/2008JC005229>, 2009.

- Dmitrenko, I. A., Rudels, B., Kirillov, S. A., Aksenov, Y. O., Lien V. S., Ivanov, V. V., Schauer, U., Polyakov, I. V., Coward, A., and Barber, D. J.: Atlantic Water flow into the Arctic Ocean through the St. Anna Trough in the northern Kara Sea, *J. Geophys. Res.: Oceans*, 120(7), 5158–5178, doi: 10.1002/2015JC010804, 2015.
- 655
- Fahrbach, E., Meincke, J., Osterhus, S., Rohardt, G., Schauer, U., Tverberg, V., and Verduin, J.: Direct measurements of volume transport through Fram Strait, *Polar Res.*, 20(2), 217–224, doi: 10.1111/j.1751-8369.2001.tb00059.x, 2001.
- Fedorov, K. N.: Physical Nature and Structure of Oceanic Fronts, *Gidrometeoizdat, Leningrad*, 296 pp., 1983 (in Russian).
- 660
- Ivanov, V. V., and Shapiro, G. I.: Formation of dense water cascade in the marginal ice zone in the Barents Sea, *Deep-Sea Res. Pt. I*, 52, 1699–1717, doi: 10.1016/j.dsr.2005.04.004, 2005.
- Ivanov, V., and Golovin, P.: Observations and modelling of dense water cascading from northwestern Laptev Sea shelf, *J. Geophys. Res.*, 112, C09003, doi:10.1029/2006JC003882, 2007.
- 665
- Ivanov, V. V., and Aksenov, E. O.: Atlantic Water transformation in the Eastern Nansen Basin: observations and modelling, *Arctic and Antarctic Research*, 1(95), 72–87, 2013 (in Russian).
- Joyce, T. M.: A note on the lateral mixing of water masses, *J. Phys. Oceanogr.*, 7(4), 626–629, 1980.
- 670
- Kolås, E., and Fer, I.: Hydrography, transport and mixing of the West Spitsbergen Current: the Svalbard Branch in summer 2015, *Ocean Sci.*, 14, 1603–1618, doi: 10.5194/os-14-1603-2018, 2018.
- Kuzmina, N. P.: On the parameterization of interleaving and turbulent mixing using CTD data from the Azores Frontal Zone, *J. Mar. Syst.*, 23(4), 285–302, 2000.
- 675
- Kuzmina, N., Rudels, B., Zhurbas, V., and Stipa, T.: On the structure and dynamical features of intrusive layering in the Eurasian Basin in the Arctic Ocean, *J. Geophys. Res.*, 116, C00D11, doi: 10.1029/2010JC006920, 2011.
- Kuzmina, N. P., Zhurbas, N. V., and Rudels B.: Structure of intrusions and fronts in the deep layer of the Eurasian Basin and Makarov Basin (Arctic), *Oceanology*, 53(4), 410–421, doi: 10.1134/S0001437013040061, 2013.
- 680
- Kuzmina, N. P., Zhurbas, N. V., Emelianov, M. V., and Pyzhevich, M. L.: Application of interleaving Models for the Description of intrusive Layering at the Fronts of Deep Polar Water in the Eurasian Basin (Arctic), *Oceanology*, 54(5), 557–566, doi: 10.1134/S0001437014050105, 2014.

- 685 Kuzmina, N. P.: Generation of large-scale intrusions at baroclinic fronts: an analytical consideration with a reference to the Arctic Ocean, *Ocean Sci.*, 12, 1269–1277, doi: 10.5194/os-12-1269-2016, 2016.
- Kuzmina, N. P., Skorokhodov, S. L., Zhurbas, N. V., and Lyzhkov, D. A.: On instability of geostrophic current with linear vertical shear at length scales of interleaving, *Izv. Atmos. Ocean. Phys.*, 54(1), 47–55, doi: 10.1134/S0001433818010097, 2018.
- 690 Marnela, M., Rudels, B., Houssais, M.-N., Beszczynska-Möller, A., and Eriksson, P. B.: Recirculation in the Fram Strait and transports of water in and north of the Fram Strait derived from CTD data, *Ocean Sci.*, 9, 499–519, doi: 10.5194/os-9-499-2013, 2013.
- Merryfield, W. J.: Intrusions in Double-Diffusively Stable Arctic Waters: Evidence for Differential mixing?, *J. Phys. Oceanogr.*, 32, 1452–1459, 2002.
- 695 Pérez-Hernández, M. D., Pickart, R. S., Pavlov, V., Våge, K., Ingvaldsen, R., Sundfjord, A., Renner, A. H. H., Torres, D. J., and Erofeeva, S. Y.: The Atlantic Water boundary current north of Svalbard in late summer, *J. Geophys. Res.-Oceans*, 122, 2269–2290, <https://doi.org/10.1002/2016JC012486>, 2017.
- 700 Pfirman, S. L., Bauch, D., and Gammelsrød, T.: The northern Barents Sea: water mass distribution and modification, in: *The Polar Oceans and Their Role in Shaping the Global Environment*, Geophysical Monograph 85, edited by: Johannessen, O. M., Muench, R. D., and Overland, J. E., American Geophysical Union, Hoboken, NJ, 77–94, 1994.
- Pnyushkov, A. V., Polyakov, I. V., Ivanov, V. V., Aksenov, Ye, Coward, A. C., Janout, M., and Rabe, B.: Structure and variability of the boundary current in the Eurasian Basin of the Arctic Ocean, *Deep-Sea Res. Pt. I*, 101, 80–97, <https://doi.org/10.1016/j.dsr.2015.03.001>, 2015.
- 705 Pnyushkov, A. V., Polyakov, I. V., Padman, L., and Nguyen An T.: Structure and dynamics of mesoscale eddies over the Laptev Sea continental slope in the Arctic Ocean, *Ocean Sci.*, 14, 1329–1347, <https://doi.org/10.5194/os-14-1329-2018>, 2018a.
- 710 Pnyushkov, A. V., Polyakov, I. V., Rember, R., Ivanov, V. V., Alkire, M. B., Ashik, I. M., Baumann, T. M., Alekseev, G. V., and Sundfjord, A.: Heat, salt, and volume transports in the eastern Eurasian Basin, *Ocean Sci.*, 14, 1349–1371, <https://doi.org/10.5194/os-14-1349-2018>, 2018b.
- Polyakov, I. V., Beszczynska, A., Carmack, E. C., Dmitrenko, I. A., Fahrbach, E., Frolov, I. E., Gerdes, R., Hansen, E., Holfort, J., Ivanov, V. V., Johnson, M. A., Karcher, M., Kauker, F., Morison, J., Orvik, K. A., Schauer, U., Simmons, H. L., Skagseth, Ø., Sokolov, V. T., Steele, M., Timokhov, L. A., Walsh, D., and Walsh, J. E.: One more step toward a warmer Arctic, *Geophys. Res. Lett.*, 32, L17605, doi: 10.1029/2005GL023740, 2005.

- 720 Polyakov, I., Timokhov, L., Dmitrenko, I., Ivanov, V., Simmons, H., Beszczynska-Möller, A.,
Dickson, R., Fahrbach, E., Fortier, L., Gascard, J.-C., Hölemann, J., Holliday, N. P., Hansen,
E., Mauritzen, C., Piechura, J., Pickart, R., Schauer, U., Walczowski, W., and Steele, M.:
Observational program tracks Arctic Ocean transition to a warmer state, *Eos Trans. AGU*,
88(40), 398–399, <https://doi.org/10.1029/2007EO400002>, 2007.
- 725 Polyakov, I. V., Alexeev, V. A., Ashik, I. M., Bacon, S., Beszczynska-Möller, A., Carmack, E.
C., Dmitrenko, I. A., Fortier, L., Gascard, J.-C., Hansen, E., Hölemann, J., Ivanov, V. V.,
Kikuchi, T., Kirillov, S., Lenn, Y.-D., McLaughlin, F. A., Piechura, J., Repina, I., Timokhov,
L. A., Walczowski, W., and Woodgate, R.: Fate of Early 2000s Arctic Warm Water Pulse,
Bulletin of the American Meteorological Society, 92(5), 561–566, doi:
10.1175/2010BAMS2921.1, 2011.
- 730 Polyakov, I. V., Pnyushkov, A., Rember, R., Ivanov, V., Lenn, Y.-D., Padman, L., and Carmack,
E. C.: Mooring-based observations of the double-diffusive staircases over the Laptev Sea, *J.*
Phys. Oceanogr., 42, 95–109, doi: 10.1175/2011JPO4606.1, 2012.
- 735 Polyakov, I. V., Pnyushkov, A. V., Alkire, M. B., Ashik, I. M., Baumann, T. M., Carmack, E. C.,
Goszczko, I., Guthrie, J., Ivanov, V. V., Kanzow, T., Krishfield, R., Kwok, R., Sundfjord, A.,
Morison, J., Rember, R., and Yulin, A.: Greater role for Atlantic inflows on sea-ice loss in the
Eurasian Basin of the Arctic Ocean, *Science*, 356, 285–291,
<https://doi.org/10.1126/science.aai8204>, 2017.
- Rudels, B.: On the mass balance of the polar ocean, with special emphasis on the Fram Strait,
Skr. Nor. Polarinst., 188, 1–53, 1987.
- 740 Rudels, B., Jones, E. P., Anderson, L. G., and Kattner, G.: On the intermediate depth waters of
the Arctic Ocean, in: *The Role of the Polar Oceans in Shaping the Global Climate*, edited by:
Johannessen, O. M., Muench, R. D., and Overland, J. E., American Geophysical Union,
Washington, DC, 33–46, 1994.
- 745 Rudels, B.: Aspects of Arctic oceanography, in *Physics of ice-covered seas*, vol. 2, edited by:
Leppäranta, M., Univ. Press, Helsinki, 517–568, 1998.
- Rudels, B., Björk, G., Muench, R. D., and Schauer, U.: Double-diffusive layering in the Eurasian
Basin of the Arctic Ocean, *J. Mar. Syst.*, 21(1–4), 3–27, doi: 10.1016/S0924-7963(99)00003-
2, 1999.
- 750 Rudels, B., Jones, E. P., Schauer, U., and Eriksson, P.: Atlantic sources of the Arctic Ocean
surface and halocline water, *Polar research*, 23(2), 181–208, doi: 10.1111/j.1751-
8369.2004.tb00007.x, 2006.

- Rudels, B., Kuzmina, N., Schauer, U., Stipa, T., and Zhurbas, V.: Double-diffusive convection and interleaving in the Arctic Ocean – Distribution and importance, *Geophysica*, 45(1–2), 199–213, 2009.
- 755 Rudels, B.: Arctic Ocean circulation, processes and water masses: A description of observations and ideas with focus on the period prior to the International Polar Year 2007–2009, *Progress in Oceanography*, 132, 22–67, doi: 10.1016/j.pocean.2013.11.006, 2015.
- Rudels, B., Korhonen, M., Schauer, U., Pisarev, S., Rabe, B., and Wisotzki A.: Circulation and transformation of Atlantic water in the Eurasian Basin and the contribution of the Fram Strait inflow branch to the Arctic Ocean heat budget, *Progress in Oceanography*, 132, 128–152, doi: 760 10.1016/j.pocean.2014.04.003, 2015.
- Schauer, U., Muench, R. D., Rudels, B., and Timokhov, L.: Impact of eastern Arctic shelf waters on the Nansen Basin intermediate layers, *J.Geophysical Res.*, 102(C2), 3371–3382, 1997.
- Schauer, U., Loeng, H., Rudels, B., Ozhigin, V. K., and Dieck, W.: Atlantic Water flow through 765 the Barents and Kara Seas, *Deep-Sea Res. Pt. I*, 49(12), 2281–2298, [https://doi.org/10.1016/S0967-0637\(02\)00125-5](https://doi.org/10.1016/S0967-0637(02)00125-5), 2002a.
- Schauer, U., Rudels, B., Jones, E. P., Anderson, L. G., Muench, R. D., Björk, G., Swift, J. H., Ivanov, V., and Larsson, A.-M.: Confluence and redistribution of Atlantic water in the Nansen, Amundsen and Makarov basins, *Ann. Geophys.*, 20, 257–273, doi: 10.5194/angeo- 770 20-257-2002, 2002b.
- Schauer, U., Fahrbach, E., Osterhus, S., and Rohardt, G.: Arctic warming through the Fram Strait: Oceanic heat transport from 3 years of measurements, *J.Geophysical Res.*, 109(C06026), doi: 10.1029/2003JC001823, 2004.
- Stern, M. E.: Lateral mixing of water masses, *Deep-Sea Res.*, 14, 747–753, doi:10.1016/S0011- 775 7471(67)80011-1, 1967.
- Swift, J. H., Jones, E. P., Aagaard, K., Carmack, E. C., Hingston, M., MacDonald, R. W., McLaughlin, F. A., Perkin, R. G.: Waters of the Makarov and Canada basins, *Deep-Sea Res. II*, 44(8), 1503-1529, doi: 10.1016/S0967-0645(97)00055-6, 1997.
- Våge, K., Pickart, R. S., Pavlov, V., Lin, P., Torres, D. J., Ingvaldsen, R., Sundfjord, A., and 780 Proshutinsky, A.: The Atlantic Water boundary current in the Nansen Basin: Transport and mechanisms of lateral exchange, *J. Geophys. Res.*, 121, 6946–6960, <https://doi.org/10.1002/2016JC011715>, 2016.
- Walsh, D., and Carmack, E.: The nested structure of Arctic thermohaline intrusions, *Ocean Model.*, 5, 267–289, doi: 10.1016/S1463-5003(02)00056-2, 2003.
- 785 Woodgate, R. A, Aagaard, K., Muench, R. D., Gunn, J., Bjork, G., B. Rudels, Roach, A. T., and Schauer, U.: The Arctic Ocean boundary current along the Eurasian slope and the adjacent

Lomonosov Ridge: Water mass properties, transports and transformations from moored instruments, *Deep-Sea Res. Pt. I*, 48(8), 1757–1792, [https://doi.org/10.1016/S0967-0637\(00\)00091-1](https://doi.org/10.1016/S0967-0637(00)00091-1), 2001.

790 Zhurbas, N. V.: On the eigenvalue spectra for a model problem describing formation of the large-scale intrusions in the Arctic Basin, *Fundamentalnaya i Prikladnaya Gidrofizika*, 11(1), 40–45, doi: 10.7868/S2073667318010045, 2018.

Zhurbas, N. V.: Estimation of Flow Rate and Thermohaline Characteristics of Atlantic Water in the Eurasian Basin, *Russian Meteorology and Hydrology*, 44, 603–612, doi: 795 10.3103/S1068373919090048, 2019.

Zhurbas, V. M., Kuzmina, N. P., Ozmidov, R. V., Golenko, N. N., and Paka, V. T.: Manifestation of subduction in thermohaline fields of vertical fine structure and horizontal mesostructure in frontal zone of Azores Current, *Okeanologiya+*, 33, 321–326, 1993.

Zhurbas, V., Elken, J., Paka, V., Piechura, J., Väli, G., Chubarenko, I., Golenko, N., and 800 Shchuka, S.: Structure of unsteady overflow in the Słupsk Furrow of the Baltic Sea, *J. Geophys. Res. – Oceans*, 117, C04027, doi:10.1029/2011JC007284, 2012.